applied sciences

MDPI

*Article*

# Experimental Study on Anti-Explosion Performance of the Different Types of Structures in Rock under the Condition of Plane Charge Explosion Loading

**Nan Ji [1,2], Xiangyun Wu [2,*], Rongguo Zhao [1,3,*], Chaochen Zhai [2], Yuefei Zhang [2] and Xiaodong Nie [1,2]**

1 School of Mechanical Engineering and Mechanics, Xiangtan University, Xiangtan 411105, China; 16637706172@163.com (N.J.)
2 Institute of Defense Engineering, AMS, PLA, Luoyang 471000, China
3 Key Laboratory of Dynamics and Reliability of Engineering Structures of College of Hunan Province, Xiangtan University, Xiangtan 411105, China
* Correspondence: 13503882599@139.com (X.W.); zhaorongguo@xtu.edu.cn (R.Z.)

**Abstract:** In this paper, the straight-wall-arch structure in the rock medium is taken as the research object, and the high-pressure plane charge loading test technology is adopted to study the anti-explosion performance of different types of structures under the explosion loading. Three types of structures, which are individually built with the high-performance reinforced concrete, the C30 reinforced concrete, and the C30 reinforced concrete with a foam concrete backfill layer as well, are tested, and the dynamic responses and damage characteristics of these structures are investigated. The test results show that under the condition of the same plane charge explosion loading, in the vault of the high-performance reinforced concrete test section appears a through-tensile crack with a largest transverse relative displacement between the two straight walls, and the composite structure test section only shows an intermittent crack at the arch foot, which represents a slight damage mode. Meanwhile the arch spring of the C30 reinforced concrete test section suffers a through-compression shear failure with a largest vertical relative displacement between the vault and the floor, which represents a moderate damage mode. Therefore, adopting the high-performance reinforced concrete, and the C30 reinforced concrete with the foam concrete backfill layer, can effectively decrease the damage degree of the rock structures. Compared with the C30 reinforced concrete, the high-performance reinforced concrete can improve the resistance of the structure by improving the structural strength and strengthening its capacity to absorb waves and energy dissipation, and the foam concrete backfill layer can significantly reduce the lateral and vertical relative displacement of the structural free surface and the peak stress of the structural inner layer. The composite structure test section of the C30 reinforced concrete with foam concrete backfill layer appears to be an excellent anti-explosion performance property.

**Keywords:** concrete structures in rock; dynamic response; damage characteristics; anti-explosion performance; plane charge explosion loading

check for updates

**Citation:** Ji, N.; Wu, X.; Zhao, R.; Zhai, C.; Zhang, Y.; Nie, X. Experimental Study on Anti-Explosion Performance of the Different Types of Structures in Rock under the Condition of Plane Charge Explosion Loading. *Appl. Sci.* **2023**, *13*, 5097. https://doi.org/10.3390/app13085097

Academic Editor: Ricardo Castedo

Received: 21 March 2023
Revised: 14 April 2023
Accepted: 17 April 2023
Published: 19 April 2023



## 1. Introduction

Due to the underground engineering structures suffering a serious damage effect under the condition of explosion loading, the resistance capacity is an important index to measure the anti-explosion performance of underground engineering structures, and improving the resistance of engineering structures is the most effective protective strategy to deal with explosion loads. Therefore, it is necessary to deeply develop the study of the dynamic response characteristics and anti-explosion performance of the structures under the explosion loading. At present, the physical similarity model test is an important method to study the anti-explosion abilities of underground engineering structures under the explosion loading. However, due to the limitations of test equipment and related technologies, the “small-scale structure tests” are usually used to test the anti-explosion resistance of prototype structures, or as an experimental validation for calibrating the theoretical calculation results, and the problems, such as boundary effects, structural influence areas, and floor reflection effects, that commonly exist in model experiments. Therefore, it is unclear whether the structural response characteristics and damage effects are consistent with prototype tests or not. Comparing with the physical similarity model test, the field high-pressure plane charge test is usually designed as an anti-explosion test for the large-scale structures or prototype structures, thus the problem of “small scale” in the similar model tests can be solved, and the peak pressure and positive pressure duration in the middle and far regions under the explosion loading can be accurately simulated. As the main structural type of underground engineering, research on the anti-explosion performance of straight-wall-arch structures is an urgent problem for the anti-explosion design and the selection of the underground engineering structures under the explosion loading.

For a long time, the underground structure has been mainly composed of a surrounding rock reinforcement layer and a reinforced concrete support structure. For a few tunnels with low resistance requirements and good surrounding rock quality conditions, the surrounding rock reinforcement layer can effectively improve the characteristics of the surrounding rock, and prevent the occurrence of fractures, falling rocks and flying rocks on the free face of the rough tunnel. Wang [1] systematically reviewed and discussed the main research on the development and engineering applications of the nonlinear stress wave propagation theory over the past half century, and applied the plane wave loading technology with high pressure, large area and controllable waveform in the rock mass, and gave the attenuation law of peak stress with propagation distance under the plane charge explosion loading. In order to study the dynamic characteristics of reinforced concrete slabs under the near-plane explosion loads, Peng [2] developed a special test device to simulate the plane charge explosion technology (PET), and successfully simulated the intensity and duration of the near-plane explosion loads in 0.1~0.4 MPa and 85~135 ms, respectively. In the research of the surrounding rock reinforcement layer, Gu [3] used a physical simulation test to study the influence of different anchorage strategies of the chamber structure under the plane charge explosion loading on the anti-explosion effect, and discovered that the locally lengthened dense anchor bolt support at the arch spring could effectively prevent or block the development of cracks in the surrounding rock and force the cracks to bypass the anchoring zone, which resulted in improving the explosion resistance capacity of the anchorage chamber. Wang [4] studied the anti-explosion performances of the two types of surrounding rock reinforcement chamber structures under the action of plane charge explosion stress waves by using explosion model test techniques, and found that the full-length bonded anchor reinforcement strategy had a better effect on reducing peak displacement than the strain and acceleration of the vault. In practical engineering applications, when the underground structure is in a poor geological and lithological environment, the surrounding rock reinforcement layer no longer satisfies the requirement of structural resistance. In order to ensure the static stability of the surrounding rock and enhance its dynamic load resistance, it is necessary to build reinforced concrete structures outside the surrounding rock reinforcement layer to improve the structural resistance. Based on the matrix force method, Fan [5] proposed a calculation method for the dynamic response of the circular tunnel lining structure, and obtained that the maximum displacement of the circular tunnel lining structure under the action of explosion seismic waves occurred at the top and bottom. When the wave impedance ratio between the surrounding rock and the lining is greater than 0.25, the influence of surrounding rock on the dynamic response of the lining structure is reduced. Chen [6] compared and analyzed the peak stress and deformation characteristics around the unlined chamber and the lined chamber under the condition of plane charge loading by using the explosion model test techniques, and found that the lining support structure was of an important technical measure to improve the resistance grade of the engineering structure.

At present, there are two main ways to improve the resistance of underground engineering structures. The first is to use the high-strength materials as the main structural materials to improve the structural strength, and the second is to backfill the soft material (energy absorbing material) between the surrounding rock and the supporting structure to weaken the intensity of explosion wave, which then indirectly results in improving the resistance of the engineering structure. The high-performance concrete has some excellent properties, such as high compressive strength, toughness and durability, which are important aspects for the development of concrete material. Thus, comparing with the C30 concrete structure, the high-performance concrete structure has many advantages in the properties of anti-explosion and anti-penetration [7–9]. A lot of research reports indicate that the addition of steel fiber reduces the risk of explosion spalling in concrete. The presence of steel fiber can bridge microcracks inside concrete, and improve the tensile strength of concrete and the overall bearing capacity of the structure [10–12]. In addition, many studies have shown that under the explosion loading, the Steel Fiber Reinforced Concrete (SFRC) exhibits better explosion resistance than the ordinary concrete, and can more effectively prevent the risk of explosion spalling [13–16]. Jiao [17] carried out an explosion test for the steel-fiber-reinforced high-strength concrete, and the results showed that the SFRC had a significant anti-seismic collapse performance effect, and its anti-seismic collapse performance mainly depended on the tensile strength of the concrete. Su [18–21] conducted some extensive static and dynamic tests for the UHP-SFRC structural members added with steel fiber, and found that the steel fiber could provide bridging action and reduce the structural crack width during the structural damage. The energy dissipation characteristics of the weak interlayer in the rock have a considerable influence on the attenuation of stress waves. Because the porosity is large, it is generally compressible. Only when the medium is compacted, the stress wave can cross the layer. The larger the porosity is, the faster the attenuation of stress waves [22]. Therefore, in order to reduce the impact load acting on the inner lining structure and reduce the vibration of the structure, a certain thickness of low-density material can be backfilled between the inner lining structure and the surrounding rock to form a composite structure with more than two layers, which can improve the internal force and deformation of the inner lining structure [23,24]. To obtain the propagation law of the compression wave generated by the explosion in the inhomogeneous stratigraphic medium, Wu [25] carried out an explosion test for a large ratio circular composite structure in the medium stiff stratigraphic medium, and found that the peak pressure of the compression wave on the wavefront was unequal in intensity, and most of the energy of the compression wave was transferred to the stiffness of the medium. When the stress wave propagates to the composite structure containing the foam concrete backfill layer, the foam concrete layer can significantly reduce the peak stress [26–30]. Li [31,32] conducted an elastic-plastic dynamic study on the multi-layer circular structure with a foam concrete backfill layer in the rock by using the calculation program, and analyzed the dynamic test and numerical calculation results of the composite structure under the action of plane shock wave load, and discussed the dynamic characteristics of the underground multi-layer circular structure and the influence of the backfill layer thickness on the dynamic response of the structural system. The optimum thickness of foam concrete layer for the wave clipping vibration reduction, and the optimum wave impedance ratio of both the surrounding rock and the backfill material, were given. The anti-explosion and seismic performances of the high-resistance concrete structure were investigated by using the plane loading test under the condition of high pressure, and the stress, deformation and vibration characteristics of the surrounding rock, backfill layer and reinforced concrete lining were obtained. By analyzing the interaction mechanism among the three different types of structures, it was found that the composite circular structure with a soft backfill layer possessed excellent explosion and impact resistance properties.

At present, due to the limitations of test cost and test technique, the research on the damage characteristics and damage mechanisms of underground engineering structures under the condition of plane charge explosion loading mainly focuses on "the small-scale physical similarity model tests". Although these tests can provide some references for the anti-explosion design of underground engineering, there is no clear certainty whether the macroscopic damage characteristics and damage mechanisms between the model tests and the prototype tests are consistent. In this paper, the prototype tests of the anti-explosion performance of the high-performance reinforced concrete structure, the C30 reinforced concrete structure and the C30 reinforced concrete structure with a foam concrete backfill composite structure in the rock medium are carried out by using the field high-pressure plane charge loading test technology, with a total charge of 384 kg. The damage characteristics and damage mechanisms of the three types of structures are investigated by observing the macro damage phenomenon and analyzing the dynamic responses of the specific structure.

## 2. Test Design and Program

### *2.1. Lithology of Test Site Area*

The stratigraphic lithology of the test site area is mainly medium-thick layered dolomitic limestone, and a small part is thin-layer dolomitic limestone. The rock mass joints are small, and have been filled with calcite veins, no weak interlayer is found, and it is a semi-hard type. A probe hole in the test site is set, and a cylindrical sample with a diameter of 50 mm and a length of 100 mm is taken for analysis. The physical and mechanical parameters of the rock in the test site are obtained through an acoustic wave test of the probe hole and a mechanical test of the specimen, as shown in Table 1.

**Table 1.** The physical parameters of the rock specimens.

| Density ($g/cm^3$) | Elastic Modulus (GPa) | Poisson's Ratio | Uniaxial Compressive Strength (MPa) | Tensile Strength (MPa) | Longitudinal Wave Velocity (km/s) | Transverse Wave Velocity (km/s) |
|---|---|---|---|---|---|---|
| 2.66 | 43.86 | 0.30 | 58.61 | 6.05 | 4.69 | 2.52 |

### *2.2. The Mix Design of Materials*

The tests for the three types of structure, which are named as the C30 reinforced concrete structure, the high-performance reinforced concrete structure and the C30 reinforced concrete with foam concrete composite structure, respectively, are designed to compare their anti-explosion performances. Among them, the C30 reinforced concrete structure is used as the benchmark structure to compare and analyze the anti-explosion performance of the high-performance reinforced concrete structure and the C30 reinforced concrete with foam concrete composite structure.

The mix design of the C30 concrete is shown in Table 2, in which sand is used as a fine aggregate with a particle size of less than 5 mm. The gravel particle size is 5~40 mm. The measured static compressive strength grade is 28 MPa.

**Table 2.** The mix design of the C30 concrete.

| Material | P.O42.5 Cement | Water-Cement Ratio | Sand | Crushed Stone | Water-Reducing Admixture |
|---|---|---|---|---|---|
| Mass ratio | 1.0 | 0.39 | 1.29 | 2.88 | 1% |

The mix design of the foam concrete is shown in Table 3. The foam agent is diluted with water at 1:20, and the foaming ratio is calculated as 30 times. The measured static compressive strength of foam concrete is 3.25 MPa.

**Table 3.** The mix design of the foam concrete.

| Material | Dry Density ($kg/m^3$) | Cement ($kg/m^3$) | Water ($kg/m^3$) | Foam Agent ($kg/m^3$) |
|---|---|---|---|---|
| Content | 750 | 625 | 312.5 | 0.913 |

The raw materials of the high-performance concrete mainly contain cement, silica fume, fly ash, quartz powder, quartz sand, nanometer mineral powder (including NS: nanometer $SiO_2$ and NC: nanometer $CaCO_3$), steel fiber, and polycarboxylate superplasticizer. The mix design of the high-performance concrete is shown in Table 4. Among them, the length of steel fiber is 20 mm and the diameter is 4 mm. The measured static compressive strength grade is 200 MPa.

**Table 4.** The mix design of high-performance concrete.

| Material | P.O42.5 Cement | Water to Binder Ratio | Quartz Sand | Quartz Powder | Microsilica | Fly ash | Water-Reducing Admixture | Steel Fiber | Nanometer Mineral Powder |
|---|---|---|---|---|---|---|---|---|---|
| Mass ratio | 1.0 | 0.16 | 1.1 | 0.3 | 0.2 | 0.1 | 1.5% | 1% | 1.5%NS + 3%NC |

### 2.3. Test Program

The explosion crater size of the plane charge loading test is 9.0 m × 5.5 m × 2.0 m, in which the height of the explosion cavity is 0.5 m. By adopting the high-pressure plane charge loading test technique, 384 kg of rock expanded ammonium nitrate explosive is designed to be arranged in the explosion cavity in the three layers. The head and tail of a single rock expanded ammonium nitrate explosive roll are connected to form a cord-like explosive roll with the same length as the explosion cavity. The cord-like explosive roll is evenly distributed in the explosion cavity in the three layers. All the cord-like explosive rolls are connected by the detonating fuse to form the initiation network, which is connected to the electric detonator. Each row of charge is detonated by detonating fuse to form a wire detonation. The cord-like charge of each layer is detonated at multiple points at the same time. The combination of line detonating and multi-point detonating ensures the formation of a quasi-plane blast wave after the explosion of each layer of explosives in the explosion cavity. The schematic of the high-pressure plane charge loading test is shown in Figure 1. The design value of the tamped backfill layer at the upper part of the formwork is 5 m, and the overburden density is about 1600 $kg/m^3$.

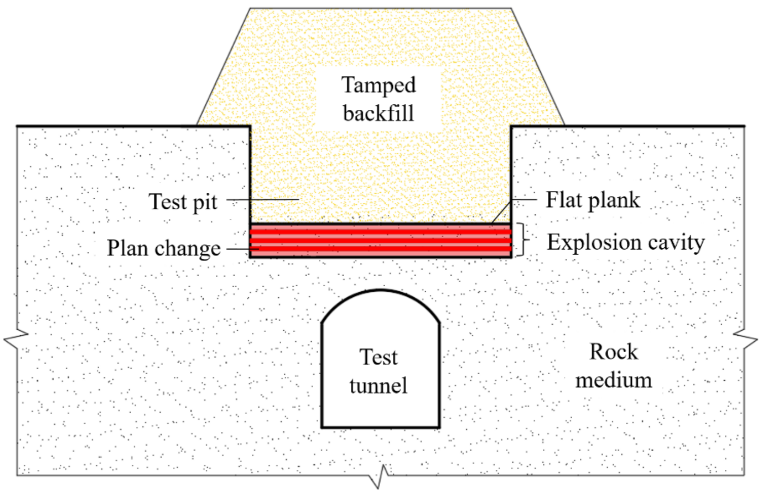


**Figure 1.** The schematic of the high-pressure plane charge loading test.

The test tunnel is 0.5 m away from the bottom of the explosion cavity. The total length of the test tunnel is 9 m. A total of 3 test sections are designed in the tunnel. Three test sections A, B and C are arranged from the structure mouth inward. Each test section is 3 m. The engineering layout of the structural test sections is shown in Figure 2. The test section A is a high-performance reinforced concrete prefabricated structure, which is constructed by way of factory prefabrication and on-site assembly. To ensure the strength of the high-performance reinforced concrete structure and convenience of transportation, it is prefabricated in two sections with the length of each section 1.5 m and thickness 0.3 m, and the two prefabricated structures are connected by using 9 high-strength bolts and concrete adhesive. The test section B was a C30 reinforced concrete structure with thickness 0.3 m, which is cast on site. The test section C is a composite structure of C30 reinforced concrete with foam concrete backfill layer, with a thickness of the C30 reinforced concrete of 0.3 m, and a thickness of the foam concrete soft backfill layer of 0.45 m. In order to ensure that the foam concrete backfill layer and the supporting structure can be closely combined, the foam concrete backfill layer is constructed by adopting the cast-in-situ method. The C30 reinforced concrete layer, as well as the high-performance reinforced concrete layer, of the inner structure in the three test sections possess the same cross-sectional size, and the horizontal length, and vertical one, and the length of free surface of the inner structure are all 1.8 m. The schematic diagrams of the cross-sectional dimensions of each test section are shown in Figure 3.

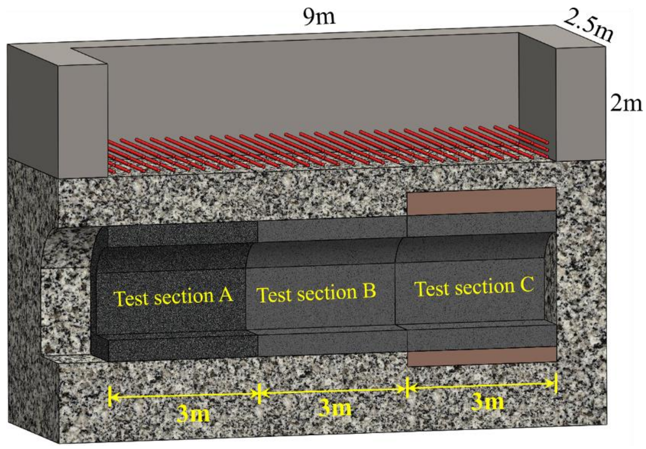


**Figure 2.** The engineering layout of the test sections.

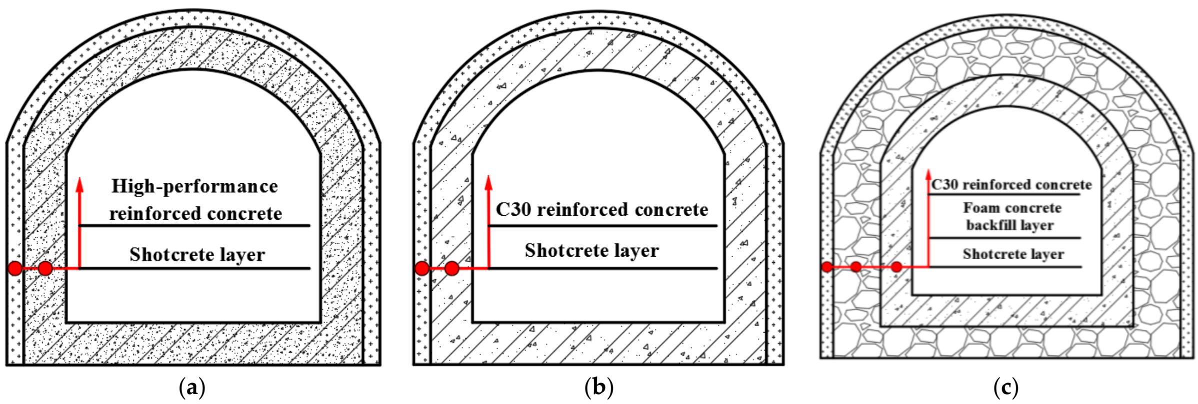


**Figure 3.** The schematic diagrams of the cross-sectional dimensions of each test section: (**a**) cross-section of test section A; (**b**) cross-section of test section B; (**c**) cross section of test section C.

In order to effectively analyze the damage effect of the structure under the plane charge explosion loading, the test measurement mainly includes the structural mechanical parameters and the structural deformations, cracks, and failure forms.

Four pressure-measuring points are designed at the bottom of the explosion cavity to measure the load at the bottom of the explosion cavity. The carbon resistance pressure sensor packaged by the flat polymer is selected as the sensor, as shown in Figure 4. The working principle of the carbon resistance pressure sensor is based on the piezoresistive effect of the composite conductive material [33]. The sensor is a flat structure, and the packaging material is the emery epoxy polymer, which has a good match of mechanical properties with the concrete and rock medium. It is considered that the fireball in the explosion cavity after the explosion probably destroy the pressure sensor and the insulated conductor, and the stress wave generated by the adjacent in-line explosive in the explosion cavity will form the Mach reflection. In order to eliminate the above adverse factors, and facilitate data collection, the strategies of setting a groove in the rock medium at the bottom of the explosion cavity, and embedding the pressure sensors and the insulated conductor as well, are adopted to shield too many interference signals. The four pressure sensors are buried in the plane Z that is parallel to the bottom surface of the explosion cavity, and 5 cm from the bottom of the explosion cavity. Since the sensor is only 5 cm away from the bottom of the explosion cavity, it can be approximately considered as the pressure at the bottom of the explosion cavity. Figure 5a is the spatial position diagram of the pressure sensors, in which the upper top surface is the bottom surface of the explosion cavity. Figure 5b is the top view of Figure 5a. Figure 5b shows the placement position of the pressure sensor on plane Z. After the pressure sensors and the wires are laid out, the interface of the sensors and the insulated conductor is lined with epoxy resin for water-proof and moisture-proof sealing treatment. The insulated conductor is laid from the side of the explosion cavity through the trench, and then fixed with plain concrete after being firmly positioned.

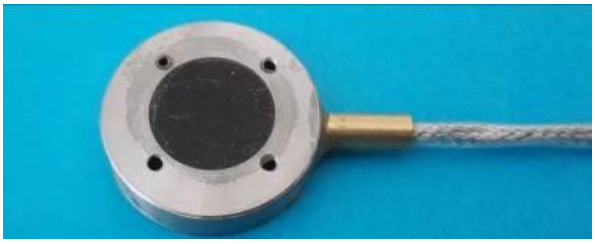

**Figure 4.** The carbon resistance pressure sensor.

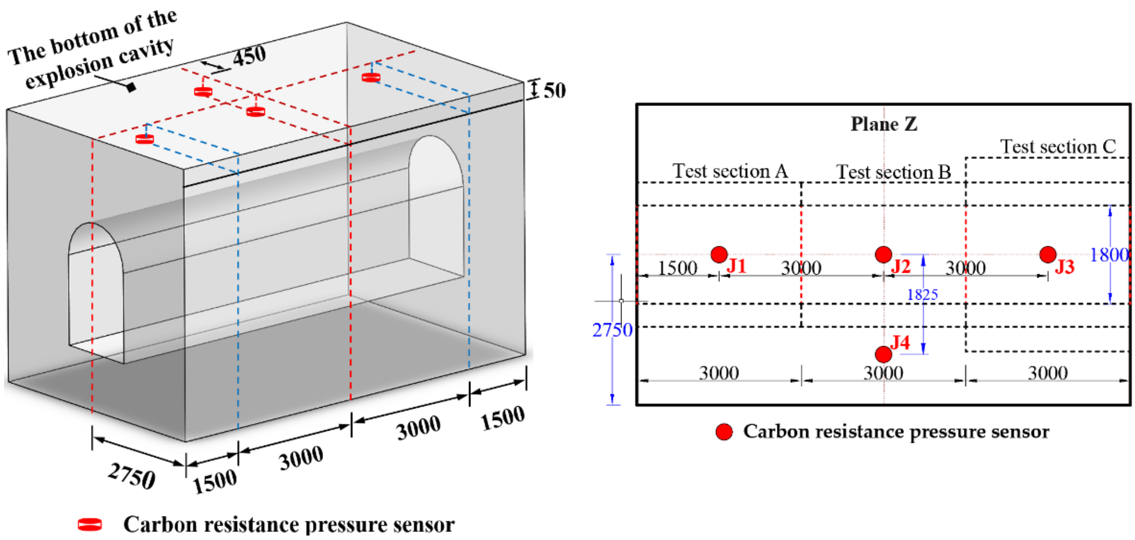


**Figure 5.** The transducer's layout at the bottom of the explosion cavity (mm): (**a**) The spatial position diagram of the pressure sensors; (**b**) the top view of the plane Z.

The central cross-section of three test sections was selected as the structural test surface, and five pressure measuring points (vault, hance, right arch spring, straight wall center, and floor center) are set on the inner layer of each structural test surface. Each measuring point is equipped with a carbon resistance pressure sensor, wherein the pressure sensors in the arch are perpendicular to the radius direction of the arch curvature, and the interface of the sensor and the insulated conductor are lined with epoxy resin for water-proof and moisture-proof sealing treatment. The DONGHUA DH5960 dynamic signal test analyzer is used for data acquisition and recording.

The two points between the left and right straight walls, and that between the vault and the floor center, are arranged in each test section to measure the transverse and vertical relative displacement of the structure under plane charge explosion loading. The ranges of the selected displacement sensors used in this research are 200 mm. The layouts of the displacement sensors are shown in Figure 6.


**Figure 6.** The internal engineering layout of the test sections.

To facilitate the measurement of the width, length and coordinates of the structural cracks after explosion, as well as the damaged parts, scope and thickness of the structure, after the construction and maintenance of the test sections are completed, the parallel marking lines are painted on the internal surface of the structure along the axial and transverse directions of the test sections, with a spacing between the marking lines of 20 cm, and the coordinates are marked, as shown in Figure 6.

## 3. Test Results and Analysis

### *3.1. The Pressures at the Bottom of Explosion Cavity*

Figure 7 shows the measured pressure time travel curve at the bottom of the explosion cavity. It can be seen from Figure 7 that approximately uniform plane waves are generated at the bottom of the explosion chamber. As shown in Table 5, the mean peak pressures at the bottom of the explosion cavity are 24.37 MPa, and the mean duration time of positive pressure is 11.84 ms. Comparing with the conventional group charges, such as the spherical charges and the cylindrical ones, the planar charges can not only simulate the peak pressure of the explosion load, but also ensure the duration time of the long-term positive pressure.

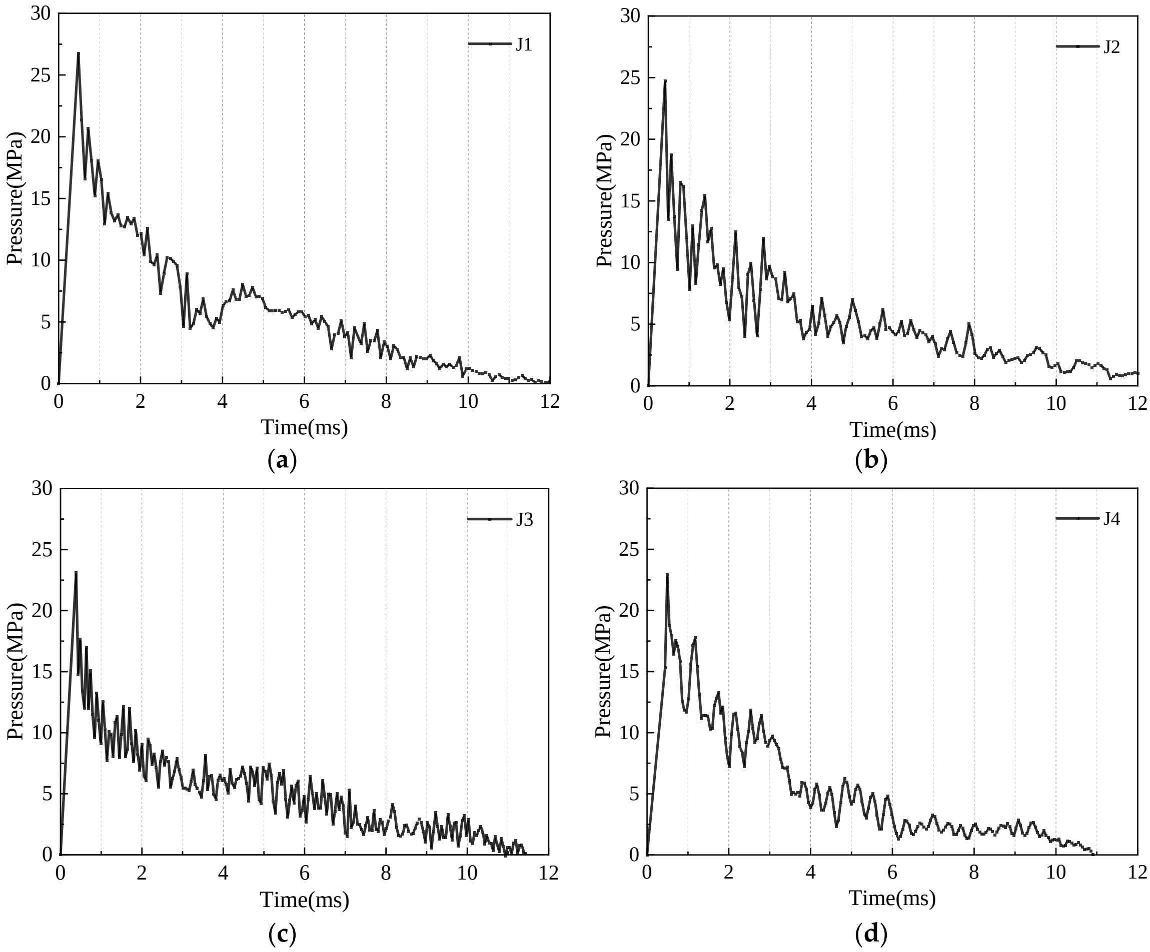


**Figure 7.** The measured pressure time travel curves at the bottom of the explosion cavity: (**a**) measuring point J1; (**b**) measuring point J2; (**c**) measuring point J3; (**d**) measuring point J4.

**Table 5.** The measured results at the bottom of the explosion cavity.

| Measuring Point | Peak Pressures (MPa) | | Duration of Positive Pressure (ms) | |
|---|---|---|---|---|
| | Measured Value | Mean Value | Measured Value | Mean Value |
| J1 | 26.74 | 24.37 | 12.27 | 11.84 |
| J2 | 24.72 | 24.37 | 12.75 | 11.84 |
| J3 | 23.11 | 24.37 | 11.44 | 11.84 |
| J4 | 22.91 | 24.37 | 10.91 | 11.84 |

### *3.2. The Description of the Macroscopic Damage Characteristics of the Structures*

The expanded photograph of the arch and straight wall of the test sections after explosion is obtained by means of segmental shooting, cropping and combination, as shown in Figure 8. From left to right, the test sections A, B and C are shown in the figure, in which the test section A is located at the mouth of the structure. By collecting and analyzing data of the test sections suffering the explosion load, the macroscopic damage characteristics of the three different types of structures are described.

The macroscopic damage phenomenon of the internal structure of test section A after enduring the explosion load is shown in Figure 9a. The width of the crack in the middle of the vault is about 5 mm, and completely connects with the bottom of the explosion cavity. However, the crack in the vault is not a continuous straight line. The crack extends from the prefabricated bolt hole to the vault. The reason is that the high-performance reinforced concrete test section is composed of the two precast sections. Although the bolt hole has been performed in a smooth engineering treatment, the stress concentration phenomenon still occurs. In addition to the influence of the material heterogeneity and inconsistent boundary conditions at the two ends of the test section, the above asymmetrical cracks are formed.

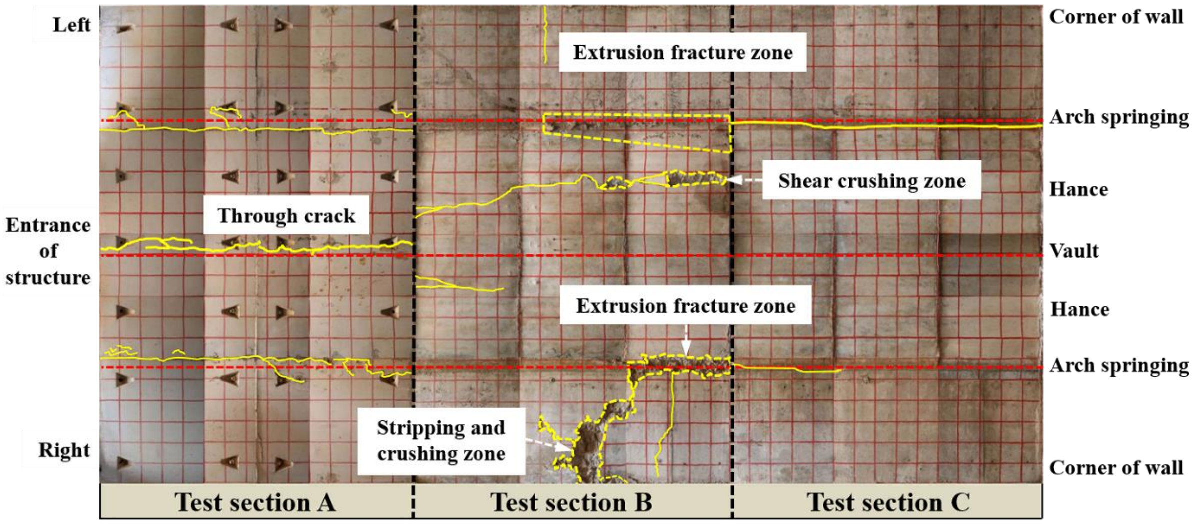


**Figure 8.** The expanded photograph of the arch and straight wall of the test sections after explosion.

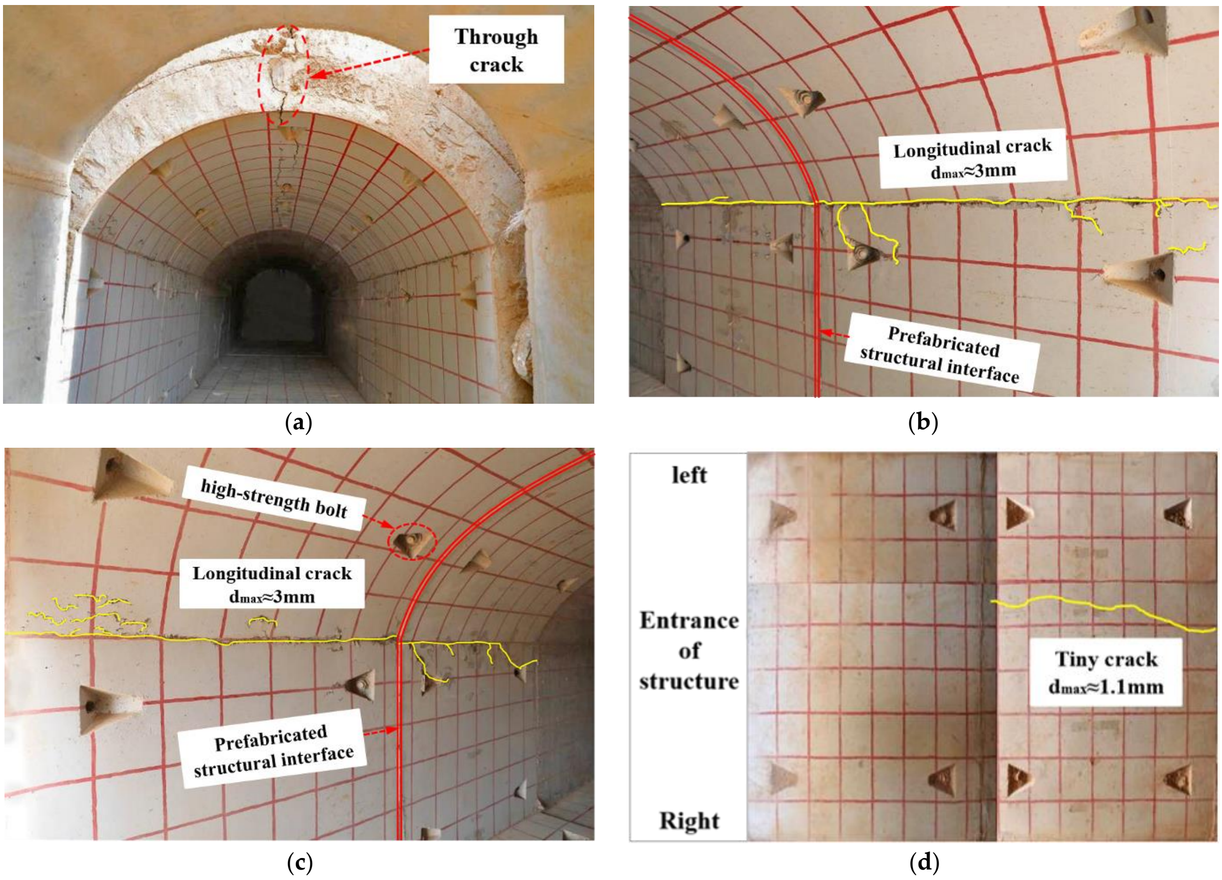


**Figure 9.** The damage state of test section A: (**a**) the photograph of the internal structure; (**b**) the damage state of the left arch spring; (**c**) the damage state of the right arch spring; (**d**) the damage state of the floor.

The high-performance reinforced concrete on the inner surface of the left and right arch feet is slightly damaged, and the left and right arch spring appears some discontinuous cracks along the thickness direction, as shown in Figure 9b,c. According to the analysis, under the condition of plane explosion wave load, the high-performance reinforced concrete firstly occurs a slight damage at the arch spring, which increases the bending moment of the vault. Under the action of reflected tensile wave, the stress characteristics of the arch change results in the appearance of an opening crack mode in the vault. Furthermore, there is no obvious damage to the straight walls on both sides. There is only a long thin crack with length 1.1 mm and 70 cm away from away from the left straight wall on the floor, which is caused by the foundation reaction and coincided with the damage position of the bottom of the explosion cavity, as shown in Figure 9d. The crack at the bottom of the explosion cavity deflects to the left, and the downward load is slightly larger. The macroscopic damage of the C30 reinforced concrete test section is shown in Figure 10, and there are no obvious cracks on the vault. Near the direction of the entrance, four small cracks with the width about 1 mm appears on both sides of the arch waist. The crack on the right spandrel extends about 90 cm from the end face of the structure. The left spandrel almost runs through the test section, especially in the second half of the test section, with the concrete shear breaking and falling, and the crack runs through the outer surface of the structure.

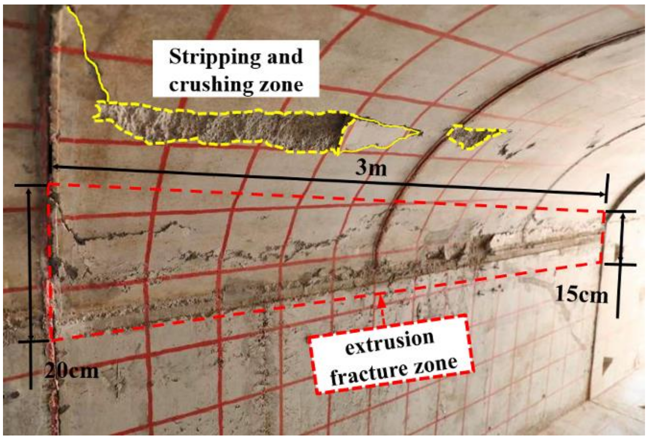


(a)

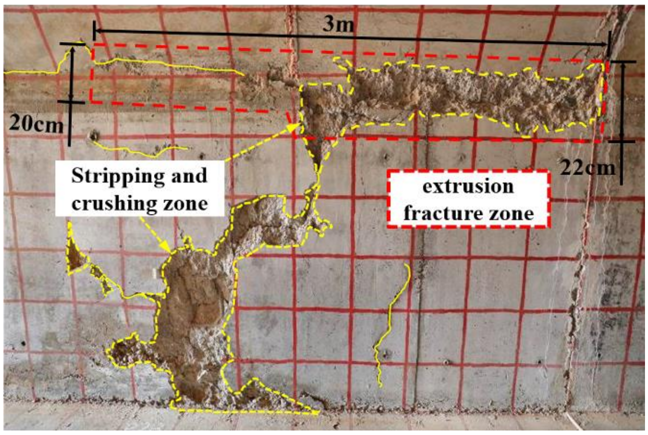


(b)

**Figure 10.** The damage states of the left arch spring and the right one: (**a**) the left arch spring; (**b**) the right arch spring.

The left arch spring appears an extrusion fracture zone, part of the concrete fall off, and there is an empty drum sound when the part that does not fall off is knocked, as shown in Figure 10a. The right arch spring emerges an extrusion fracture zone within 1 m of the inner end face, with a width of 20 cm, and the concrete is crushed and dropped, as shown in Figure 10b. The left straight wall only produces a vertical micro-crack at 125 cm away from the outer end of the structure. From the perspective of the concrete falling area, the damage on the left side is relatively slight, while the straight wall on the right side is seriously damaged, resulting in a large stripping and crushing zone.

There is a main crack with a width of 3 mm through the floor of test section B in the middle of the structure. A crack with a length of tens of centimeters appears at both the ends of the crack, which is caused by the foundation restraint reaction force. In addition, there is a transverse crack in the middle of the left side, which is connected with the damage area of the left straight wall, as shown in Figure 11a.

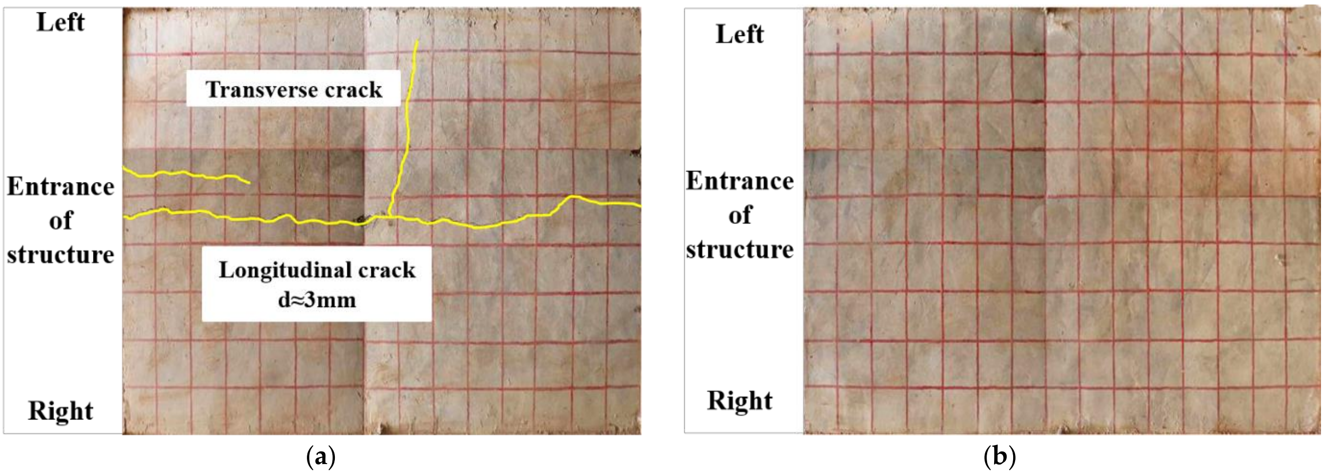


**Figure 11.** The damage state of the floor: (**a**) test section B; (**b**) test section C.

The macroscopic damage of the composite test section of the C30 reinforced concrete with the foamed concrete backfill layer is shown in Figure 9. The tiny cracks appear at the left and right arch spring, the longitudinal full-length cracks appear at the left arch spring, and the length of the right arch spring is about 90 cm from the inner end face. There is no obvious damage to the floor, as shown in Figure 11b. The test section C is slightly damaged.

Simultaneously, in order to determine the damage grades of the three structures based on the previous classification criteria of the damage grades that are classified as total damage, severe damage, moderate damage and slight damage, and combining with the macroscopic damage phenomenon and damage characteristics of the three structures, the damage grade and damage characteristics of the three different types of structures are given, as shown in Table 6.

**Table 6.** The damage grades and damage characteristics of the test sections.

| Test Section | Structural Material | Damage Characteristics | Damage Mechanism | Damage Grade |
| --- | --- | --- | --- | --- |
| A | High-performance reinforced concrete | The maximum width of the vault is about 5 mm. Cracks along the thickness direction appear at the left and right arch spring, and a tiny crack appears in the floor. | Tensile failure Compression shear damage | Slight damage |
| B | C30 reinforced concrete | There are no obvious cracks in the vault. The concrete of the hance is stripped, resulting in the through cracks and shear damage zone. The arch spring has an extrusion fracture zone, part of the concrete falls off. A through crack with a width of about 3 mm appears on the floor. | Part of compression shear damage Splitting tensile | Moderate damage |
| C | C30 reinforced concrete with foam concrete | Tiny cracks appear at the left and right arch spring. | Part of compression shear damage | Slight damage |

### 3.3. *The Structural Dynamic Response Analysis*

Table 7 shows the measured peak stress at each measuring point in the structural inner layer. It can be seen from Table 7 that the peak stress distribution at each measuring point in the inner layer of the same structure is not uniform. The maximum peak stress lies at the measuring point in the inner layer of the arch spring, and the stress concentration is obvious. When the strain value caused by peak stress exceeds the deformation resistance of the structure, the arch spring is more likely to be damaged relative to the other positions of the structure.

**Table 7.** The peak stress of each measured point in the structural inner layer.

| Measuring Point | C30 reinforced Concrete Test Section | High-Performance Reinforced Concrete Test Section | | Composite Structure Test Section | |
|---|---|---|---|---|---|
| | Peak Stress (MPa) | Peak Stress (MPa) | Stress Reduction Effect Factor | Peak Stress (MPa) | Stress Reduction Effect Factor |
| Vault | 22.88 | 15.81 | 30.9% | 8.74 | 61.8% |
| Hance | 33.72 | 19.78 | 41.3% | 8.89 | 73.6% |
| Arch Spring | 42.31 | 52.74 | −24.6% | 22.56 | 46.7% |
| Straight Wall | 29.45 | 22.21 | 24.6% | 12.98 | 55.9% |
| Floor | 15.71 | 11.36 | 27.7% | 9.63 | 38.7% |

In order to quantitatively compare the advantages and disadvantages of the three types of structures, a dimensionless stress reduction effect factor is defined, that is

$$b = (S_i - S_{\Sigma i})/S_i$$

where $S_i$ is the peak stress at point $i$ in the reference structure test section that is named as the C30 reinforced concrete test section, $S_{\Sigma i}$ is the peak stress at the corresponding measuring point $i$ in the comparison structure test section $\Sigma$, and $b$ is the stress reduction rate of the measuring point $i$ in the comparison structure test section to the reference structure test section. The closer the value $b$ tends to 1, the better the stress reduction effect of each measuring point in the comparison structure test section is.

On the basis of Table 7, the peak stress of each measuring point on the cross section of the straight-wall-arch structures is fitted to obtain the distribution rule of the peak stress along the key measuring points of the cross-section of the arch structure, as shown in Figure 12. It can be seen from Figure 12 that, comparing with the C30 reinforced concrete test section, the peak stress values of the inner layer of the high-performance reinforced concrete test section, and the composite structural test section in the vault, the hance, the straight wall midpoint and the floor midpoint, all show a decreasing tendency. The peak stress of the inner layer of the floor in the C30 reinforced concrete test section is 15.71 MPa, and the attenuation effect factors of the high-performance reinforced concrete test section and the composite structural test section are 27.7% and 38.7%, respectively. Although the three types of structural test sections do not achieve the structural compression shear damage states, the three types of structural tests show the characteristics of uplift and extension failure on the floor. This is mainly caused by the diffraction when the plane compression wave propagates to the free surface of the structure, and the diffraction wave and the compression wave propagating to the floor are superimposed. When the stress of the reflected tensile wave exceeds the allowable dynamic tensile value of the structure, the floor will be pulled and cracked. On the whole, the floors of the three test sections bear relatively uniform loads transmitted by the two straight walls, and the floors basically show the characteristics of symmetrical damage and bending damage.

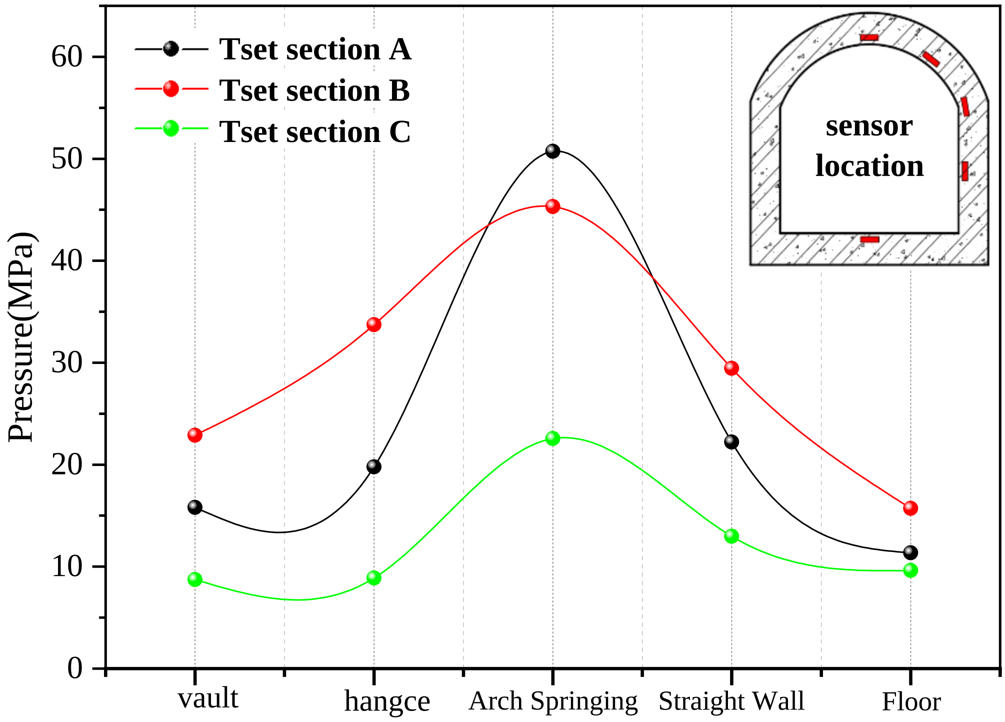


**Figure 12.** The peak stress tendency curve of the measured points in test sections.

Comparing with the C30 reinforced concrete test section, the stress reduction effect factor at the arch spring of the high-performance reinforced concrete test section is −24.6%. The reason is that in the clamped arch stress system, the arch spring first produced a stress concentration. When the peak stress at the arch spring of the C30 reinforced concrete structure reaches 42.31 MPa, the structure produces a compression shear damage, while the high-performance reinforced concrete test section has a high structural stiffness, and the energy of the compression wave is transmitted more in a medium with high stiffness, which makes the stress concentration at the arch spring of the structure more remarkable, with the measured peak stress reaching 52.74 MPa. However, the high-performance concrete materials improve the brittleness of the structure and enhance the fracture toughness and impact resistance of the structure, so that only intermittent cracks form at the arch spring. It is found that damage of the arch spring is mainly caused by the phenomenon of stress concentration at the arch-wall junction caused by the compressive shear load. If the high-performance reinforced concrete test section is damaged, with the continuous propagation of microcracks at the arch spring, the steel fiber will be pulled out of the matrix. As the interfaces between the steel fiber and the matrix are numerous and irregular, the paths of microcrack initiation and propagation are more complex, and the action of bonding and friction between the two interfaces results in the intensifying of the internal energy consumption of the structure. Comparing with the C30 reinforced concrete test section, the peak stress values in the inner layer of the vault, the hance, the straight wall midpoint and the floor midpoint of the high-performance reinforced concrete test section decrease about 30.9%, 41.3%, 24.6% and 27.7%, respectively. Therefore, the high performance reinforced concrete test section improves the structural resistance by enhancing the structural strength and increasing the energy dissipation.

Comparing with the C30 reinforced concrete test section, the peak stress values in the inner layer of the vault, the hance, the arch spring, the straight wall midpoint and the floor midpoint of the composite structural test section decrease individually about 61.8%, 73.6%, 46.7%, 55.9% and 38.7%, respectively, which indicates that the foam concrete soft backfill can significantly reduce the peak stress in the inner layer of the structure. The foam concrete, as a porous lightweight material, has a wave impedance much lower than that of the surrounding rock and the C30 reinforced concrete structures. When the stress waves propagate to the composite structures with mismatched wave impedance, the stress waves at adjacent interfaces form multiple reflections and transmissions, which dissipate certain energy in this process. Furthermore, when the stress wave propagates inside the foam concrete, the free surface formed by the honeycomb holes causes multiple reflections, refractions and superpositions of the stress waves, and the energy from the explosion shock waves further decays. In addition, the measured static compressive strength of the foam concrete is 3.25 MPa; when the explosion stress wave propagates to the energy dissipation layer of the foam concrete, the impact load exceeds the dynamic compressive strength of the foam concrete, and most of the explosion energy is absorbed by the plastic deformation of the foam concrete soft backfill medium, which results in a weakening of the impact load transmitted to the structure. The peak stress tendency curve of the measuring points in the composite structural test section is gentle, as shown in Figure 12. Under the action of a dynamic load, the foam concrete soft backfill layer can slow down the deformation of the surrounding rock reinforcement layer. Simultaneously, it can reduce the pressure, isolate the vibration, and improve the stress distribution around the supporting structure, thus indirectly enhance the structural resistance of the composite structural test section.

By analyzing the stress response of the structural inner layer of the three different types of structures, it is found that among these three structures, the composite structure possesses the most effective wave absorption and energy dissipation effects. After the foam concrete energy dissipation layer is added to the composite structure test section, the mean attenuation rate of the peak stress of the structure achieves 55.34%. Based on the research results of existing scholars on the anti-explosion performance of underground structures, the attenuation rate of the foam concrete backfill layer to the peak stress is summarized in Table 8.

**Table 8.** The attenuation rate of the foam concrete backfill layer to the peak stress.

| No. | Author | Location of Measuring Points | Attenuation Rate |
|---|---|---|---|
| 1 | Li, H.Q. [26] | Mean value of measurement points | 68% |
| 2 | Tang, D.G. [27] | Mean value of measurement points | 95% |
| 3 | Zhang, B. [28] | vault | 98% |
| 4 | Tian, Z.M. [29] | Mean value of measurement points | 89.24~93.42% |
| 5 | Chen, R.L. [30] | vault | 90% |
| 6 | Ji, N. (This article) | vault<br>Mean value of measurement points | 61.8%<br>55.34% |

The time–history curves of the measured vertical relative displacement between the vault and the floor and the measured transverse displacement between the left and right straight walls for the structures, after enduring the explosion load, are shown in Figure 13. It can be seen from Figure 13 that the vertical relative displacements of the test sections of the C30 reinforced concrete, the high-performance reinforced concrete, and the composite structure are individually 52.9 mm, 31.9 mm and 19.9 mm, and the transverse ones are 26.8 mm, 46.48 mm and 3.27 mm, respectively. Under the same loading conditions, the measured relative displacement and residual displacement of the three types of structural test sections are different. Among them, for the high-performance reinforced concrete test section and the C30 reinforced concrete one, after suffering the peak values of vertical and transverse relative displacements, the plastic deformations of the structure produce irrecoverable residual displacements, while the residual displacement of the composite structural test section is small, and the total displacement mainly appears as an elastic deformation.

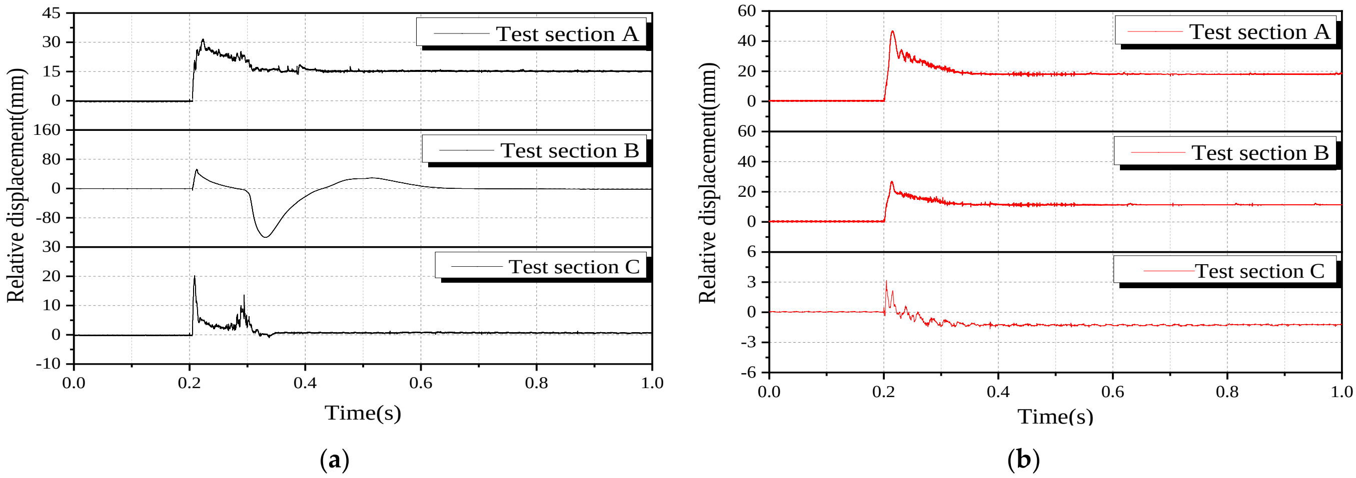


**Figure 13.** The time–history curves of the relative displacement of the structures: (**a**) the vertical relative displacement; (**b**) the transverse relative displacement.

In Figure 13a, there is an abnormal phenomenon in the data after the peak vertical relative displacement value in the C30 reinforced concrete test section, because it is known from the macro failure phenomenon of the structure that downward displacement occurs at the vault, while the time–history curve of the vertical relative displacement shows no residual displacement. Considering the serious damage of the structure, it is very likely that the slungshot produced by the peeling affected the test system; therefore, only the first peak displacement is used as a reference. As shown in Figure 13a, the vertical relative displacement of the high-performance reinforced concrete test section is 31.6 mm, which is 40.3% less than that of the C30 reinforced concrete test section. Based on the analysis of the macroscopic damage phenomenon of the C30 reinforced concrete test section, the compression shear damage zone appears at the hance and arch spring of the C30 reinforced concrete test section and the structural damage is serious, while the internal surface of the high-performance reinforced concrete test section is complete, with a vertical crack with a maximum width of 5 mm at the vault, and an intermittent crack at the arch spring. It can be seen that the vertical relative peak displacement of the high-performance reinforced concrete test section is the result of the combined action of the arch spring crack and the structural deformation, while that of the C30 reinforced concrete test section is generated by the hance crack, the arch spring plastic hinge and the structural deformation. Therefore, the vertical relative displacement of the C30 reinforced concrete test section is greater than that of the high-performance reinforced concrete one. As shown in Figure 13b, the transverse relative displacement of the high-performance reinforced concrete test section is 46.6 mm, which is 94.0% higher than that of the C30 reinforced concrete one. Under the same plane explosion loading, due to the tensile cracks in the vault of the high-performance reinforced concrete test section, it can be seen that the dynamic resistance strength of the vault exceeds the allowable value. At this time, the arch-wall junction bears a large outward horizontal thrust. However, the arch spring of the C30 reinforced concrete test section produces a compression shear damage and forms a plastic hinge, and the hance also produces a compression shear damage zone. The stiffness of the arch decreases, and the horizontal thrust transmitted from the arch to the arch-wall junction decreases. Therefore, the phenomenon increased the transverse relative displacement of the high-performance reinforced concrete test section appears. Comparing with the C30 concrete, various physical and mechanical properties of the high-performance concrete are improved, and the structural strength and resistance to deformation are increased. As the transverse relative displacement between two straight walls is large, the structure only produces intermittent cracks at the arch spring, which belongs to a lower damage grade compared with the C30 reinforced concrete structure.

The vertical relative displacement of the composite structure is 19.9 mm, which is 37.0% less than that of the C30 reinforced concrete test section, and the transverse relative displacement is 3.27 mm, which is 93.0% less than that of the C30 reinforced concrete test section. It can be seen from Figure 13 that the lateral residual displacement of the test section of the composite structure has a minus relative displacement of 1.5 mm. Combining with the peak stress at the straight wall, the straight wall has not entered the plastic deformation stage, so it is impossible to produce a minus relative displacement. However, considering that the composite structure produces some microcracks at the arch spring, and the foam concrete layer between the surrounding rock reinforcement layer and the structural layer is also broken, the foam concrete is not strong enough to resist the minus relative displacement. Therefore, the micro cracks at the arch spring cause a minus displacement of 1.5 mm in the composite structure. When the impact load is transmitted to the composite structural test section, due to the existence of the foam concrete soft backfill layer, the foam concrete possesses the properties of wave absorption and energy dissipation, which results in reducing the load impulse to the structure. Furthermore, the measured static compressive strength of foam concrete is only 3.25 MPa, after damage to the surrounding rock, the foam concrete on the upper part of the arch structure will be crushed and compacted to cushion the impact load on the structure, and finally only some tiny cracks will be produced at the arch spring. Therefore, the foam concrete has an excellent energy dissipation effect, the vertical and horizontal relative displacements of the composite structure are small, and the composite structure has a better anti-explosion performance and less effect of injury.

### *3.4. Discussion for the Test Results*

In this paper, the macroscopic damage phenomenon and damage mechanism of the structure are obtained by using the plane charge explosion loading technique. Compared with the C30 concrete materials, the utilization of high-strength materials and the foam concrete energy-absorbing materials can effectively improve the resistance of underground structures.

(1) In terms of the research test methods, reference [3,4] uses a scaled test with a small charge, while this paper innovatively uses a field high-pressure plane charge explosion loading test technique with a total charge of 384 kg of TNT to carry out the explosion resistance performance test of prototype underground structures. In order to compare and study the anti-explosion resistance performance of different types of structure, three test sections are designed at the bottom of the explosion chamber to match the requirements of the plane wave loading. This designed one-shot test method controls the variables in the explosion loading test, and saves on the cost of the test.

(2) With regards to the structural study aspects, the C30 reinforced concrete structure is taken as the reference test section, while the high-performance concrete structure and the composite structure are designed as comparative test sections to investigate the anti-explosion performances of the three different types of structure. For references [28–32], the similar simulation tests were adopted, and the attenuation rate of the foam concrete backfill layer to peak stress reached more than 65% due to the installation of bolts in the reinforcement layer of the surrounding rock, which was better than the mean peak stress attenuation rate of 55.34% in this paper.

Due to the large scale of the test, high requirements of the test site, poor test repeatability, difficulty in testing, and other adverse factors, in order to study the anti-explosion performance of the underground structures under the plane charge explosion loading conditions more systematically, some relevant studies should be conducted on the antiknock performance of structures with different backfill materials and bolts in the later stage, so as to provide technical support for the anti-explosion designs of the underground prototype engineering structures under the plane wave explosion loading.

## 4. Conclusions

In order to study the damage characteristics, dynamic responses and damage mechanisms of different types of underground structures in rock medium under the action of the plane charge explosion, a prototype test for three types of straight-wall-arch structures under the plane charge loading was carried out. The conclusions of this research are as follows:

(1) From the perspective of the structural macroscopic damage phenomenon, under the same plane charge explosion loading, the damage characteristics of the three types of structural test sections are significantly different. From the analysis of structural damage grade and damage degree, the damage of the C30 reinforced concrete structure belongs to a medium damage mode, while that of the high-performance reinforced concrete structure and the composite structure is classified as a slight damage mode, and the overall damage degree of the composite structure is weak. Comparing with the C30 reinforced concrete structure, the high-performance reinforced concrete structure and the composite one have excellent levels of anti-explosion performance, both of which can effectively reduce the damage grade.

(2) From the stress response analysis of the structural inner layer, the peak stress at the arch spring of the high-performance reinforced concrete structure is greater than that of the C30 reinforced concrete structure, while the peak stress values at the inner layer of the vault, the hance, the straight wall midpoint, and the floor midpoint are less than that of the C30 reinforced concrete structure. The high-performance concrete improves the resistance of the structure by enhancing the structural strength and increasing the energy dissipation. The foam concrete soft backfill layer reduces the maximum peak stress of the structural inner layer, and can reduce pressure, isolate vibration, and improve the stress distribution around the supporting structure, thus indirectly improving the structural resistance of the composite structure.

(3) From the analysis of the relative displacement response of the internal surface of the structure, the vertical relative displacement of the high-performance reinforced concrete test section is smaller than that of the C30 reinforced concrete test section, while the transverse relative displacement is larger than that of the C30 reinforced concrete test section. However, brittle damage does not occur in the structure. The vertical and transverse relative displacement of the composite structure are smaller than that of the high-performance reinforced concrete structure and the C30 reinforced concrete structure, and the composite structure has a better anti-explosion performance and less effect of injury.

**Author Contributions:** Conceptualization, X.N.; methodology, N.J. and R.Z.; software, N.J.; validation, N.J. and X.W.; formal analysis, N.J.; investigation, C.Z. and Y.Z.; resources, X.W. and Y.Z.; data curation, N.J.; writing—original draft preparation, N.J.; writing—review and editing, N.J.; visualization, N.J.; supervision, X.W. and R.Z.; project administration, X.W.; funding acquisition, X.W. All authors have read and agreed to the published version of the manuscript.

**Funding:** This research was supported by the Postgraduate Scientific Research Innovation Project of Hunan Province (CX20200648).

**Institutional Review Board Statement:** Not applicable.

**Informed Consent Statement:** Not applicable.

**Data Availability Statement:** The data used to support the findings of this study are available from the corresponding author upon request.

**Conflicts of Interest:** The authors declare no conflict of interest.

## References

1. Wang, L.L.; Ren, H.Q.; Yu, J.L.; Zhou, F.H.; Wu, X.Y.; Tang, Z.P.; Hu, S.S.; Yang, L.M.; Dong, X.L. Development and application of the theory of nonlinear stress wave propagation. *Chin. J. Solid Mech.* **2013**, *34*, 217–240. [CrossRef]
2. Peng, Q.; Zhou, D.Y.; Wu, H.; Ma, L.L.; Fang, Q. Experimental and numerical studies on dynamic behaviors of RC slabs under long-duration near-planar explosion loadings. *Int. J. Impact Eng.* **2022**, *160*, 104085. [CrossRef]

3. Gu, J.C.; Chen, A.M.; Xu, J.M.; Zhao, H.L.; Zhang, X.Y.; Gu, L.Y.; Ming, Q.Z. Model test study of failure patterns of anchored tunnel subjected to explosion load. *Chin. J. Rock Mech. Eng.* **2008**, *27*, 1315–1320. [CrossRef]
4. Wang, G.Y.; Gu, J.C.; Chen, A.M.; Xu, J.M.; Zhang, X.Y. Research on explosion resisting performance of tunnels reinforced by fully bonded rock bolts in model test. *Rock Soil Mech.* **2010**, *31*, 107–112. [CrossRef]
5. Fan, P.X.; Wang, M.Y.; Feng, S.F.; Li, J.; Wang, D.R. Dynamic response of deep-buried circular tunnel to explosion seismic wave. *Chin. J. Rock Mech. Eng.* **2013**, *32*, 671–680. [CrossRef]
6. Chen, A.M.; Gu, J.C.; Xu, J.M.; Kong, F.L.; Ming, Q.Z. Model test study of tunnel mechanical characteristics under plane charge explosion. *Rock Soil Mech.* **2011**, *32*, 2603–2608. [CrossRef]
7. Maca, P.; Sovjak, R.; Konvalinka, P. Mix design of UHPFRC and its response to projectile impact. *Int. J. Impact Eng.* **2014**, *63*, 158–163. [CrossRef]
8. Ellis, B.D.; Dipaolo, B.P.; McDowell, D.L.; Zhou, M. Experimental investigation and multiscale modeling of ultra-high-performance concrete panels subject to blast loading. *Int. J. Impact Eng.* **2014**, *69*, 95–103. [CrossRef]
9. Yi, N.H.; Kim, J.H.; Han, T.S.; Cho, Y.G.; Lee, J.H. Blast-resistant characteristics of ultra-high strength concrete and reactive powder concrete. *Constr. Build. Mater.* **2012**, *28*, 694–707. [CrossRef]
10. Wu, D.H.; Li, Z.W.; Li, J.L.; Peng, B.; Shen, H. Study on mechanical properties of the basalt fiber-rubber granular concrete under triaxial stress condition and its application. *Appl. Sci.* **2020**, *10*, 8540. [CrossRef]
11. Zhang, Q.; Zhang, W.; Fang, Y.; Huang, X. Experimental study on mechanical properties of high performance hybrid fiber concrete for shaft lining. *Appl. Sci.* **2021**, *11*, 7926. [CrossRef]
12. Tang, C.W. Special issue on advances in high-performance fiber-reinforced concrete. *Appl. Sci.* **2022**, *12*, 8723. [CrossRef]
13. Zhang, P.; Kang, L.Y.; Wang, J.; Guo, J.J.; Ling, Y.F. Mechanical properties and explosive spalling behavior of steel-fiber-reinforced concrete exposed to high temperature—A review. *Appl. Sci.* **2020**, *10*, 2324. [CrossRef]
14. Varona, F.B.; Baeza, F.J.; Bru, D.; Ivorra, S. Influence of high temperature on the mechanical properties of hybrid fibre reinforced normal and high strength concrete. *Constr. Build. Mater.* **2018**, *159*, 73–82. [CrossRef]
15. Li, Y.; Pimienta, P.; Pinoteau, N.; Tan, K.H. Effect of aggregate size and inclusion of polypropylene and steel fibers on explosive spalling and pore pressure in ultra-high-performance concrete (UHPC) at elevated temperature. *Cem. Concr. Compos.* **2019**, *99*, 62–71. [CrossRef]
16. Zheng, W.; Luo, B.; Ying, W. Compressive and tensile properties of reactive powder concrete with steel fibres at elevated temperatures. *Constr. Build. Mater.* **2013**, *41*, 844–851. [CrossRef]
17. Jiao, C.; Sun, W.; Gao, P. Study on steel fiber reinforced high strength concrete subjected to blast loading. *Eng. Mech.* **2008**, *25*, 158–166.
18. Su, Y.; Li, J.; Wu, C.; Wu, P.; Li, Z.X. Effects of steel fibres on dynamic strength of UHPC. *Constr. Build. Mater.* **2016**, *114*, 708–718. [CrossRef]
19. Su, Y.; Li, J.; Wu, C.Q.; Wu, P.T.; Tao, M.; Li, X.B. Mesoscale study of steel fibre-reinforced ultra-high performance concrete under static and dynamic loads. *Mater. Des.* **2017**, *116*, 340–351. [CrossRef]
20. Liu, J.; Wu, C.Q.; Su, Y.; Li, J.; Shao, R.Z.; Chen, G.; Liu, Z.X. Experimental and numerical studies of ultra-high performance concrete targets against high-velocity projectile impacts. *Eng. Struct.* **2018**, *173*, 166–179. [CrossRef]
21. Li, J.; Wu, C.Q.; Hao, H.; Wang, Z.Q.; Su, Y. Experimental investigation of ultra-high performance concrete slabs under contact explosions. *Int. J. Impact Eng.* **2016**, *93*, 62–75. [CrossRef]
22. Fang, Q.; Qian, Q.H. The dynamic interaction between stress wave and the underground structure with the soft-backfill liner. *Explos. Shock. Waves.* **1988**, *8*, 289–298.
23. Zhao, Y.X.; Wang, L.G. Dynamic analysis of underground round structure under explosion load. *Chin. J. Appl. Mech.* **1997**, *14*, 69–72.
24. Shi, S.Q.; Liu, R.H.; Wang, M. Researches of performance of new-type composite structure of steel plate-foamed aluminium-steel plate in abating explosion shock wave. *Chin. J. Vib. Shock.* **2008**, *27*, 143–146. [CrossRef]
25. Wu, X.Y.; Zhao, Y.X.; Ren, H.Q.; Li, H.Q.; Fang, Q.; Zhao, X.B. On basic way to dramatically increase the bearing capacity of underground engineering in rock mass. *Chin. J. Rock Mech. Eng.* **2003**, *22*, 261–265. [CrossRef]
26. Li, H.Q.; Lu, F.Y.; Wu, X.Y.; Zhao, Y.X.; Ren, H.Q. Study on regulation of the stress wave propagation in rock-mass with compound structures. *Chin. J. Rock Mech. Eng.* **2003**, *22*, 1832–1836. [CrossRef]
27. Tang, D.G.; Wang, K.M.; He, H.C.; Wu, H.X.; Qu, X. Energy dissipation mechanism of foamed concrete backfill layers in underground tunnels. *J. PLA. Univ. Sci. Technol. Sci. Ed.* **2006**, *7*, 365–370. [CrossRef]
28. Zhang, B.; Xu, J.Y.; Li, L.; Lin, W. Analysis of anti detonational property of foam concrete backfill layers in underground compound structure. *Sichuan Build. Sci.* **2010**, *36*, 135–138. [CrossRef]
29. Tian, Z.M.; Chen, F.N. Research on high resistance composite circular structure under dynamic load of high pressure explosion. *J. Nanjing Eng. Inst.* **1996**, *11*, 13–18.
30. Chen, R.L.; Dong, Q.; Yu, B.B.; Li, K.; Zhang, W.K.; Chen, X.H.; Zhang, X.C. Numerical research on anti-explosion capacity of foam concrete composite structure in underground openings under close-in explosion. *Chin. J. Comput. Mech.* **2019**, *38*, 267–277. [CrossRef]
31. Li, H.Q.; Zhang, S.; Ou, Y.K.Y. Dynamic response analysis of underground multi-layer cylindrical structures in rocks. *Chin. J. Rock Mech. Eng.* **2012**, *31*, 3503–3507.

32. Li, H.Q.; Wu, X.Y.; Li, Y.C. Analysis of the anti-explosion structures model of the underground compound cylindrical structures. *Chin. J. Rock Mech. Eng.* **2005**, *24*, 643–648.
33. Gebbeken, N.; Greulich, S.; Pietzsch, A. Hugoniot properties for concrete determined by full-scale detonation experiments and flyer-plate-impact tests. *Int. J. Impact Eng.* **2006**, *32*, 2017–2031. [CrossRef]